European Commission

JRC TECHNICAL REPORT

Inter-laboratory comparison of Computational Fluid Dynamics codes for PEM fuel cell modelling

Deliverable: B.2.4 Final report on CFD benchmarking

Bednarek, T, Tsotridis, G

2021

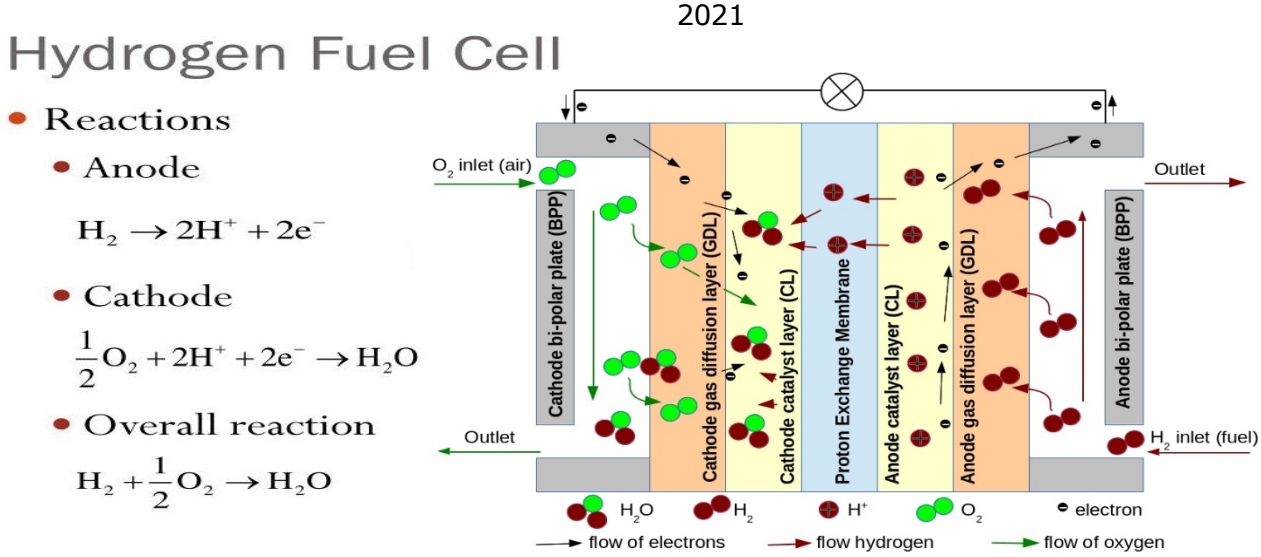

Joint Research Centre

EUR 30703 EN

Contact information
Name: Tomasz Bednarek
Address: European Commission, Joint Research Centre (JRC), Westerduinweg 3, NL-1755 LE Petten
Email: Tomasz.Bednarek@ec.europa.eu
Tel.: +31 224565447

EU Science Hub
https://ec.europa.eu/jrc

JRC124900

EUR 30703 EN

PDF ISBN 978-92-76-37770-2 ISSN 1831-9424 doi:10.2760/291664

Luxembourg: Publications Office of the European Union, 2021

How to cite this report: Bednarek T., Tsotridis G., *Inter-laboratory comparison of Computational Fluid Dynamics codes for PEM fuel cell modelling*, EUR 30703 EN, Publications Office of the European Union, Luxembourg, 2021, ISBN 978-92-76-37770-2, doi:10.2760/291664 (online), JRC124900.

Contents

Acknowledgments

The work described in this report was carried out under the framework contract between the Directorate-General (DG) Joint Research Centre (JRC) of the European Commission and the Fuel Cells and Hydrogen 2 Joint Undertaking (FCH 2 JU). The JRC contractual activities are summarised in the FCH 2 JU Multi-Annual Work Programme[1]. This report is the Deliverable B.2.4 of the annual rolling plan 2017[2].

Authors

Tomasz Bednarek

Georgios Tsotridis

[1] available online at: https://www.fch.europa.eu/sites/default/files/MAWP%20final%20version_endorsed%20GB%2015062018%20%28ID%203712421%29.pdf, pp 31.

[2] available online at: https://www.fch.europa.eu/sites/default/files/FCH2%20JU%202017%20AWP%20and%20Budget_FINAL-20122016-Clean%20%28ID%202892681%29_0.pdf, pp 86.

Abstract

An inter-laboratory comparison of Computational Fluid Dynamics (CFD) codes exercise for Polymer Electrolyte Membrane (PEM) fuel cell modelling was performed to assess modelling accuracy. Since PEM fuel cell models require a multi-physics approach involving many different phenomena, a simple comparison with experimental polarisation curves is not sufficient for the identification of the individual sources of errors the simulation software. Therefore, this report presents a methodology based on the comparison of partial simulation results.

The report introduces first the list physical models available for the simulation of fuel cell phenomena. It describes then in details reference numerical test cases. Finally, it provides an example of application showing that by this approach, it is possible to verify any simulation software for PEM fuel cells, including commercial systems, without access to the source code.

1 Introduction

The structure of the report is the following: the objective of the study is presented in Chapter 2, the results of the inventory of all the physical models available is summarised in Chapter 3 and further detailed in Annex A. The test cases developed by JRC are explained in Chaper 4 and the results are compared and analysed in Chapter 5.

The list of participants invited to contribute to the CFD codes benchmarking exercise is presented in Table 1.

Table 1 List of invited participants

Organisation	Contact person(s)
European Commission, Joint Research Centre (JRC)	Georgios Tsotridis, Tomasz Bednarek
AVL List GmbH	Reinhard Taschl, Clemens Fink
Zentrum für Sonnenenergie- und Wasserstoff-Forschung Baden-Württemberg (ZSW)	Simon Enz
Deutsche Zentrum für Luft- und Raumfahrt (DLR)	Thomas Jahnke
COMSOL AB	Henrik Ekström
Robert Bosch GmbH	Andreas Haeffelin
Le Commissariat à l'énergie atomique et aux énergies alternatives (CEA)	Arnaud Morin, Bolahaga Randrianarizafy
Università degli Studi di Salerno (UNISA)	Cesare Pianese, Pierpaolo Polverino
Aalborg Universitet	Torsten Berning

2 Objective and methods

The usual way of validation of simulation software consists of its comparison with experimental data. Such a comparison shows whether the constitutive laws used in modelling correctly reflect reality. However, for complex systems such as fuel cells, the verification of the many internal quantities (i.e. partial pressures of reactant species, permeability of diffusion layers, local temperature, resistance of internal components etc.) is very challenging. This significantly hinders to analyse, understand and resolve possible divergences between the results of simulations and experimental data. More, in some specific cases errors due to programming mistakes may cancel each other leading to false conclusion that numerical model correctly reflects real experiment. Therefore, the first phase of a simulation software validation should be the verification of the applied constitutive laws and interfaces among them, so that the fuel cell modelling code is free from implementation mistakes.

The overarching objective of the inter-laboratory comparison of CFD codes in PEM fuel cell modelling is to establish a set of test cases for validation of the constitutive laws as implemented in the simulation codes. Using the proposed reference test cases, a user of simulation software will be able to validate against theory any modelling software for PEM fuel cells, including commercial software, even without access to their source code.

In this respect, the JRC started a series of actions to facilitate this objective. The first action performed was an inventory of the models for the simulation of fuel cell phenomena used by the participants. A *reference benchmarking test case 1*, covering all aspects of PEM fuel cells, was then proposed by JRC.

In a following stage, a *benchmarking test case 2* was proposed as a modification of first case in order to assess the accuracy of the simulation of two specific contributions: the reaction kinetics and the proton conduction in ionomer. Therefore, the *reference test case 2* validates the modelling of the catalyst layer performance, namely the Hydrogen Oxidation Reaction (HOR) in the anode, Oxygen Reduction Reaction (ORR) in the cathode and losses due to proton conduction by the ionomer in the catalyst layers (anode and cathode sides).

The results of PEM fuel cell simulations are compared in terms of:

- velocity distribution in the gas channels,
- concentration of gas species in both anode and cathode fuel cell compartments, namely: gas channels, gas diffusion layers and catalyst layers,
- temperature distribution across the active area at catalyst layers and gas diffusion layers, both, anode and cathode,
- hydration of the membrane,
- protonic potential distribution in ionomer (anode and cathode catalyst layers and membrane,
- electronic potential at catalyst layers, gas diffusion layers and bi-polar plates, both anode and cathode, *and*
- in-plane current density distribution (anode and cathode).

3 Physical models used for PEM fuel cell modelling

The overview of all the physical models used for simulations of fuel cell operation in this benchmarking exercise is presented in Table 2. The physical models are grouped per fuel cell component, namely bi-polar plates (BPP), gas channels (GCH), gas diffusion layer (GDL), micro-porous layer (MPL), catalyst layer (CL), membrane (MEM). Each modelled phenomenon (mass convection, mass diffusion, electric conduction, heat transfer, proton conduction, gas-liquid (water vapour-water) phase change and electro-chemical reactions) is described by the appropriate governing equations and corresponding source terms which account for internal boundary conditions between the fuel cell components.

Details of the physical models used in the simulations are presented in Appendix A.

Table 2 Overview of physical models per fuel cell component used in simulations using CFD codes. Numbers in brackets correspond to equations in Appendix A.

		MEM	Anode CL			Cathode CL			MPL		GDL		GCH	BPP
			ionomer	carbon support	pores	ionomer	carbon support	pores	carbon particles	pores	fibres	pores		
Electron transport		–	–	Laplacian (20)	–	–	Laplacian (20)	–	Laplacian (20)	–	Laplacian (20)	–	–	Laplacian (4)
Proton transport		Electric equilibrium of H^+ (34)	Electric equilibrium of H^+ (34)	–	–	Electric equilibrium of H^+ (34)	–	–	–	–	–	–	–	–
Gas reactants	**O_2**	–	–	–	N-S with Darcy (8) Species eq. (10)	–	–	N-S with Darcy (8) Species eq. (10)	–	N-S with Darcy (8) Species eq. (10)	–	N-S with Darcy (8) Species eq. (10)	N-S (1) Species equilib. (2)	–
	H_2	–	–	–	N-S with Darcy (8) Species eq. (10)	–	–	N-S with Darcy (8) Species eq. (10)	–	N-S with Darcy (8) Species eq. (10)	–	N-S with Darcy (8) Species eq. (10)	N-S (1) Species equilib. (2)	–
Water	**vapour**	'	–	–	N-S with Darcy (8) Species eq. (10)	–	–	N-S with Darcy (8) Species eq. (10)	–	N-S with Darcy (8) Species eq. (10)	–	N-S with Darc (8)y Species eq. (10)	N-S (1) Species equilib. (2)	–
	liquid	-	Transport eq. (45)	–	Darcy (31)	Darcy (31)	–	Darcy (31)	–	Darcy (31)	–	Darcy (31)	N-S (1)	–
	dissolved	Osmotic and backflow (37)	Osmotic (37)	–	–	Osmotic (37)	–	–	–	–	–	–	–	–
Heat transfer		Conduction (48)	Conduction term in (18)		Convection term in (18)	Conduction term in (18)		Convection term in (18)	Conduction term in (18)	Convection term in (18)	Conduction term in (18)	Convection term in (18)	Convection (3)	Conduction (5)

Source: JRC, 2017

4 The reference test cases

The inter-laboratory comparison of CFD codes effort requires the establishment of a reference computational geometry and input parameters. The operating conditions correspond to those contained within the **EU Harmonised Operating Conditions for Automotive Applications** [1]. A typical MEA size of 25 cm^2 with single serpentine flow field is considered. As agreed with the participants of the exercise, in an effort to simplify the numerical solution and to minimise the effects of channel geometry, the "single serpentine cell" is approximated by a "single straight channel" of equivalent length. Such a channel configuration decreases the effects of flow field shape and simultaneously allows for comparison of results obtained from different numerical models with analytical solution results. The numerical values of input data correspond to real materials used in fuel cell testing.

The following modelling assumptions have been made:

- The external electrical circuit is modelled by applying appropriate boundary conditions to anode and cathode bi-polar plate (BPP) terminals. The applied load corresponds to galvanostatic operation mode, namely fixed electric current is applied.
- Side walls of the numerical model are assumed as symmetric in order to reduce the effects of boundaries.
- Fuel (hydrogen) and oxidant (air) are considered to be ideal gases. Therefore, the diffusion of species follows the multicomponent principles applicable to ideal gas mixtures.
- Microporous and catalyst layers (MPL and CL) are modelled as single homogeneous sub-domains. The catalyst loading is defined by the active surface ratio [m^{-1}].
- Water condensation occurs only in the porous sub-domains (GDL and CL). Therefore, a two-phase simulation is performed only in GDL and CL sub-domains. The liquid water that is produced and evacuated to the gas channel is homogenised. The liquid water takes the velocity of the surrounding gas, hence the gas flow profile is not affected by the existence of water droplets.

It should be clearly noted that in this study, as in many other similar studies, the open circuit voltage V^{OC} is an input to the CFD code. This requires calculation of V^{OC} using the Nernst equation for given operating conditions prior to the modelling.

A description of the input data used in the *reference test case 1* is given in Appendix B.

The *reference test case 1* is very demanding for a simulation software as in a single simulation run all crucial physical phenomena appear, namely: significant gradients of reactant concentrations, a relatively large volume fraction of condensed water and consequential gas density gradients in the anode compartment. Additionally, the total length of the fuel cell model (1250 mm) implies a large computational mesh, which is challenging for numerical solvers.

Despite using the same input data and geometry, the results of the *reference test case 1* simulation obtained by participants of the exercise were significantly different, hence were of very difficult analysis. Due to the complexity of the PEM fuel cell numerical model (Section 4) and the large-scale computational domain, it was impossible to distinguish differences arising from the use of different implementations of physical models and those, which may stem from inevitable numerical errors.

Therefore, the *reference test case 1* was abandoned, and learning from it the *reference test case 2* was defined allowing for an assessment of the different components contribution to the final loss of modelling accuracy, specifically to compare and validate the contribution of the fuel cell reaction kinetics to the results of the simulation. In order to minimise the effect caused by the gas inlet humidity, the concentration gradients in the reactants and liquid water that are known to affect the reactant diffusion through the GDL, the following modifications are introduced:

- The length of the channel is reduced to 80 mm in order to reduce computational efforts.
- A constant flow of both reactants is set to be equivalent to stoichiometries 10.0 at 1.0 Acm^{-2} current density to obtain a uniform species distribution along with efficient removable of product water.
- Fully humidified reactants (100% relative humidity, RH) at the inlets to avoid membrane dry out and ensure a sufficiently high and uniform membrane protonic conductivity.

The details of the *reference test case 2* are presented in Appendix C.

5 Results of the *reference test case 2* on catalyst performance

The usual way of benchmarking CFD-code results is by using reference experimental data. In this study, we compare the PEM fuel cell modelling results. This approach provides a verification method of simulation codes, which allows for identification of mistakes or bugs in the software. The following example shows how CFD inter-laboratory comparison exercises helped to improve the modelling software of two participants in the project.

There are two participants contributing to the exercise with the *reference test case 2*. Since both participants use the same constitutive laws and the same input data, it is expected that the differences in obtained results come only from numerical errors (rounding and truncation). Therefore, the obtained results should match each other with rather high accuracy. Polarisation I-V curves provided by two participants obtained according to the conditions specified in Appendix C, are presented in Figure 1.

At first glance, it could be concluded from Figure 1A that the I-V curves match each other very well and that any differences might be due to numerical errors. However, a close look in Figure 1B shows that there are differences reaching 35 mV (2nd important digit) at current density 0.4 A cm^{-2} between the simulation results provided by Participant 1 and Participant 2. It is seen also, that the difference in results increases with increasing current density, indicating that reasons of diverging results are not due to typical numerical errors (rounding or truncation), but very likely there are some mistakes in implementation of constitutive laws.

Figure 1 (A) Polarisation curves provided by benchmarking exercise participants according to conditions specified in Appendix C. (B) Zoom plot shows low current density region indicated in (A).

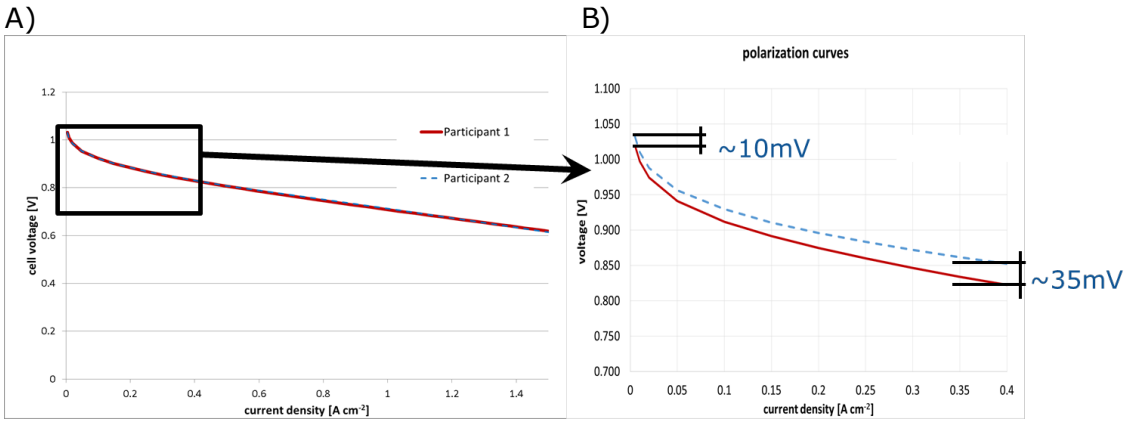

Source: JRC, 2017

To identify the reason for the discrepancy shown in Figure 1B, the polarisation curve was divided into its contributions, namely: equilibrium voltage, activation overpotential, ionic overpotential and electronic overpotential (Figure 2). The calculated overpotentials were then compared separately.

A comparison of the activation, ionic and electronic overpotentials is presented in Figure 3.

Figure 2 Split of polarisation I-V curve provided by Participant 1 into overpotentials.

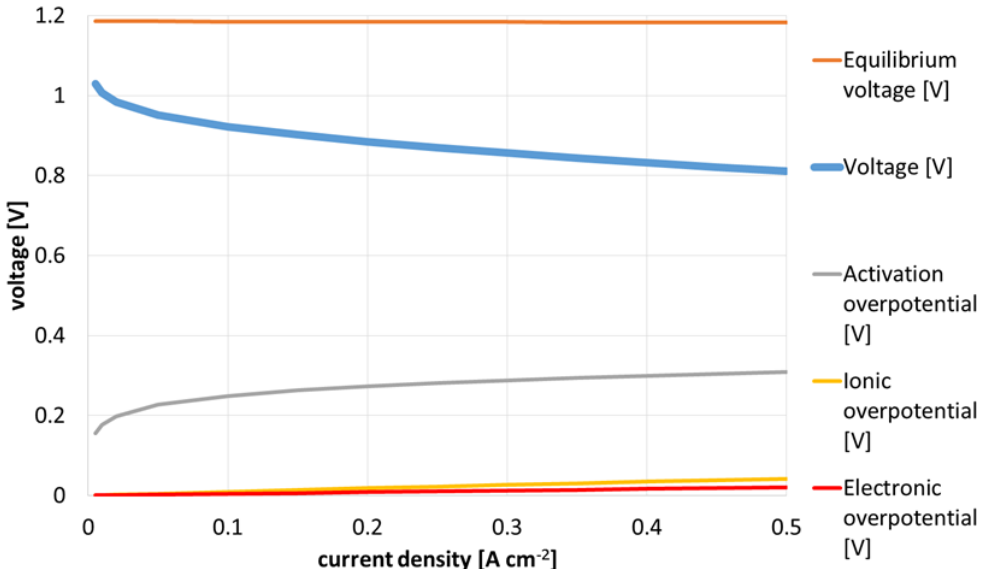

Voltage = Equilibrium voltage – activation – ionic - electronic

Source: JRC, 2017

Figure 3 Comparison of simulation results: overpotentials of the polarisation I-V curves presented in Figure 1.

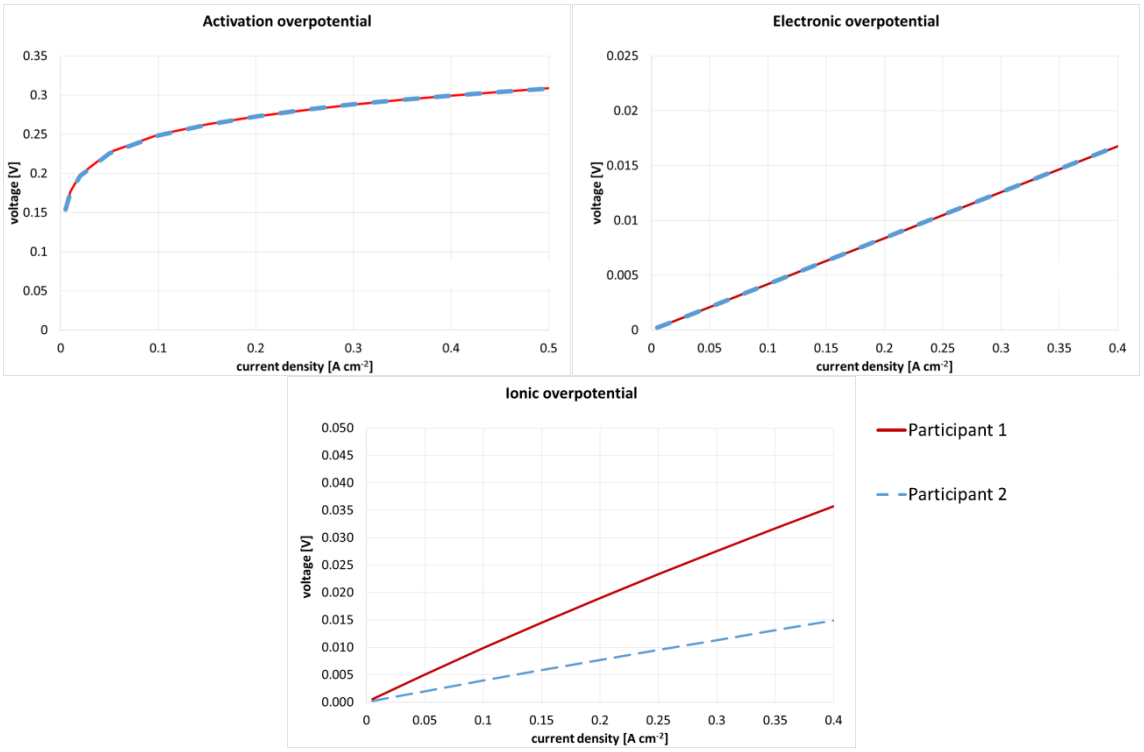

Source: JRC, 2017

It can be seen in Figure 3 that the activation and electronic overpotentials provided by the participants match each other well. However, there is a significant difference in the ionic overpotential. The ionic overpotential contains contributions arising from both the anode and cathode catalyst layers. Therefore, the ionic overpotential was split into anode and cathode ionic potentials (potential difference between MEM and GDL) as presented in Figure 4.

Figure 4 Results of simulations provided by participants: (A) anode and (B) cathode ionic overpotentials.

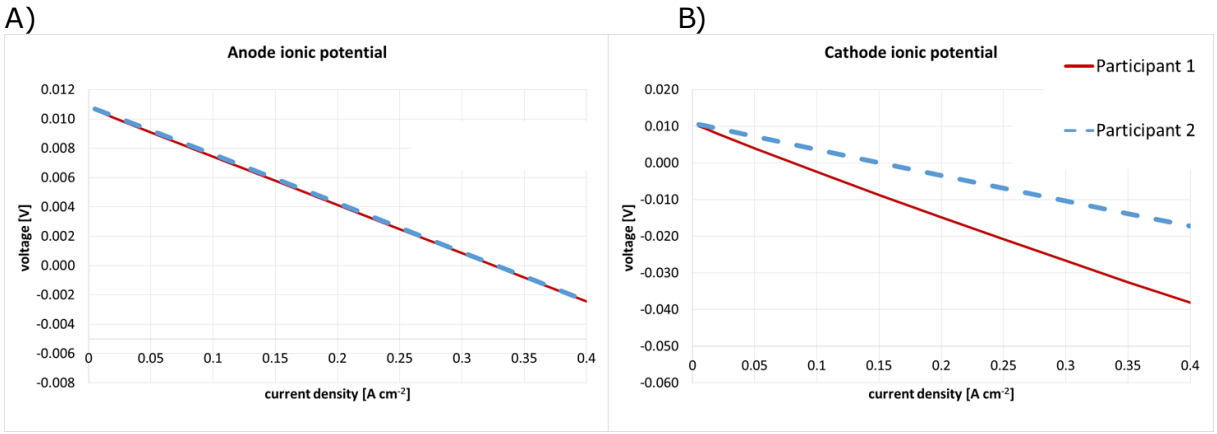

Source: JRC, 2017

In Figure 4 can be seen that differences appear to be only due to the cathode ionic potential. Since the deviation is proportional to the current density (Figure 4B) this suggests that the calculation of the ionic conductivity in the cathode CL is incorrect, corresponding to Eq. (37), see Appendix A.

In fact, both participants (Participant 1 and Participant 2) have found a software bug in their codes related to Eq. (37) in Appendix A. Participant 2 has identified the bug and corrected the mistake, however Participant 1 was not able to correct the software bug because it did not have access to the software source code.

Figure 5 Result of simulations before and after the software update by Participant 2.

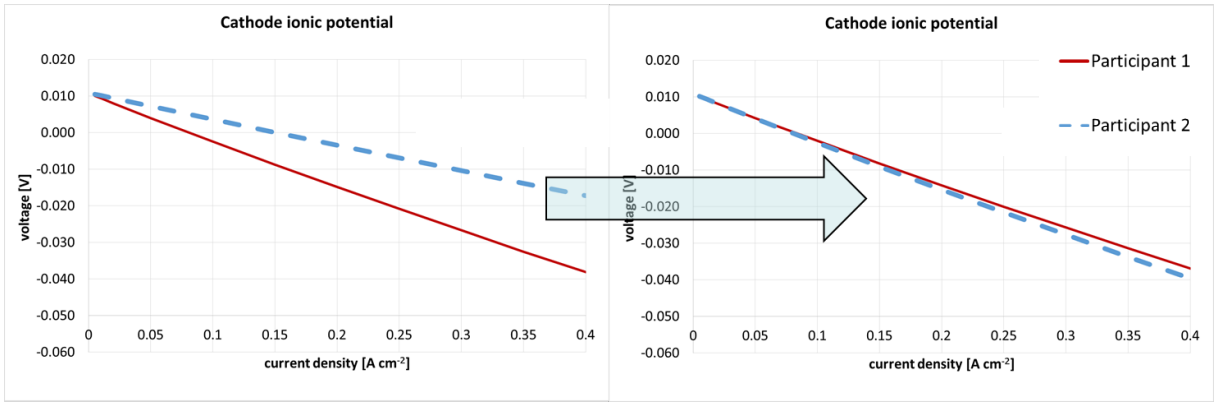

Source: JRC, 2017

6 Conclusions and outlook

The purpose of the present study was to develop a number of test cases in order to compare the results of different numerical codes, modelling the performance of a single PEM fuel cell. The results were obtained when using the same input physical values, geometry and boundary conditions. To characterise the performance of the PEM fuel cell, a polarisation curve test was chosen. The numerical codes were required to evaluate the polarisation curve using the *reference test case 1*, integrating all fuel cell related phenomena.

The results of the *reference test case 1* provided by participants of the exercise were significantly different. Due to the complexity of the numerical model it was impossible to identify the differences arising from the employed physical models from those associated numerical errors. Therefore, a *reference test case 2* was proposed to evaluate the contributions of reaction kinetics, minimising the effects of reactants delivery, temperature, pressure and material properties of the fuel cell components.

The evaluation of the modelling results of the *reference test case 2* led to the discovery of a number of mistakes in the codes. Hence, the verification of the software was performed in details, accounting internal model parameters that could not be measured during real experiment. As a result, the implementation of the physical model into simulation software becomes more trustworthy and can be next validated against real experiments.

The work described in this report is just as a first step, focussing on the reaction kinetics region of the polarisation curve. It should to be completed by similar work dedicated to the other regions of interest, namely those limited by ohmic and mass transport. For the ohmic region, additional reference test cases should be established to examine the effects of membrane hydration on its protonic resistance, as well as the effects of the electronic conductivity of fuel cell components and contact resistances. For examining the third region of the polarisation curve where mass transport limitation dominate, another reference test case should investigate losses due to reactant diffusion through GDL thickness and the effects of liquid water accumulation.

References

[1] E.L. Cussler, Diffusion. Mass Transfer in Fluid Systems, Cambridge University Press, Cambridge, 2009.

[2] A.Z. Weber, R.L. Borup, R.M. Darling, P.K. Das, T.J. Dursch, W. Gu, D. Harvey, A. Kusoglu, S. Litster, M.M. Mench, R. Mukundan, J.P. Owejan, J.G. Pharoah, M. Secanell, I. V Zenyuk, J. Electrochem. Soc. 161 (2014) F1254.

[3] R.F. Mann, J.C. Amphlett, B.A. Peppley, C.P. Thurgood, J. Power Sources 161 (2006) 775.

[4] H. Wu, X. Li, P. Berg, Electrochim. Acta 54 (2009) 6913.

[5] T.E. Springer, M.S. Wilson, S. Gottesfeld, J. Electrochem. Soc. 140 (1993) 3513.

[6] A.Z. Weber, J. Newman, Adv. Fuel Cells 1 (2007) 47.

[7] T.E. Springer, T.A. Zawodzinski, S. Gottesfeld, J. Electrochem. Soc. 138 (1991) 2334.

[8] T. Berning, M. Odgaard, S.K. Kær, J. Power Sources 196 (2011) 6305.

List of figures

List of tables

Annexes

Appendix A Details of physical models used in PEM fuel cell simulations

Table 3 List of used symbols.

a	Water activity
b	User defined exponent
C_i	Mass concentration of specie i
D_k^{eff}	Effective diffusivity of specie k in porous media
D_{gl}	Empirical diffusion coefficient for condensation and evaporation of water
D_i	Diffusion coefficient of specie i
D_{ij}	Binary diffusion coefficient
D_λ	Diffusion coefficient for water dissolved in ionomer
e^-	Electron
E_i	Activation energy
EW	Membrane equivalent weight
F	Faraday constant
h	Enthalpy
$\mathbf{i}$, i	Current and its magnitude
$\mathbf{i}_\mathrm{p}$	Protonic current
J	Volumetric current density
j^{ex}	Exchange current density
j^{ref}	Reference current density
K	Permeability
k	Effective thermal conductivity
K_r	Relative permeability due to water saturation effect
M	Molar mass
N	Number of considered species
n	Number of electrons taking part in chemical reaction

n_d	Dimensionless osmotic drag coefficient
p	Pressure
p_0	Atmospheric pressure
p_c	Capillary pressure
p_i	Partial pressure of specie i
p_l	Pressure of liquid phase
p_{sat}	Saturation pressure
R	Universal gas constant
s	Liquid water saturation
S_e	Volumetric source term, electric current source
S_{gl}, S_{gd}, S_{ld}	Mass exchange source tern between different phased of water: gas-liquid, gas-dissolved in ionomer, liquid-dissolved in ionomer
S_h	Volumetric source term, Joule heating
S_λ	Volumetric source term, water dissolved in ionomer
S_s^k	Volumetric source term, source of specie k
S_u	Volumetric source term, body force
t	Time
T	Temperature
$U_0^{an,cat}$	Half potentials for anode and cathode catalysts
$\mathbf{v}$	Flow velocity
$\mathbf{V}$	Diffusion velocity
x, y, z	Spatial dimensions
X_i	Mole fraction of specie i
X_i^{ref}	Reference mole fraction of specie i
$\alpha_{an}, \alpha_{cat}$	Anode and cathode respectively, electron exchange coefficient
β	Reaction symmetric factor
ε	Porosity

ϵ	Volume fraction of ionomer
ϕ	Electric potential
Γ	Factor accounting volume fraction and tortuosity of ionomer
γ_{an},γ_{cat}	Anode and cathode, respectively, reactant concentration exponents
γ	Average surface of a liquid water droplet
γ_{gd}, γ_{ld}	Water mass exchange rate constants between phases: gas-dissolved in ionomer and liquid-dissolved in ionomer respectively
η	Overpotential
λ	Membrane water content
$\mu, \bar{\mu}$	Dynamic viscosity, average dynamic viscosity
θ	User defined constant
$\rho, \bar{\rho}$	Density, average density
σ_{eff}	Effective electric conductivity
ζ	Electrocatalyst surface area, ECSA

Gas channels

A Newtonian fluid is considered for mass transport modelling. The liquid water is accounted as a homogenous fine mist in a gas phase. Henceforth, the Navier-Stokes (N-S) equation (momentum diffusion balance) for compressible fluids without body forces is used to describe the transport of gas and liquid phases in the gas channels, namely:

$$\frac{\partial}{\partial t}(\bar{\rho}\mathbf{v}) + \nabla \cdot (\bar{\rho}\mathbf{v}\mathbf{v}) = \nabla \cdot (\bar{\mu}\mathbf{v}) - \nabla p, \quad (1)$$

where $\mathbf{v}$ is velocity vector of the respective liquid-gas mixture, p is absolute pressure of the respective liquid-gas mixture, $\frac{\partial}{\partial t}$ is the time derivative operator, ∇ is the gradient operator of the canonical space variables (x,y,z), $\nabla = \left[\frac{\partial}{\partial x}, \frac{\partial}{yx}, \frac{\partial}{\partial z}\right]^T$, superscript ^{T} denotes transpose and $\nabla \cdot = \frac{\partial}{\partial x} + \frac{\partial}{\partial y} + \frac{\partial}{\partial z}$ is the divergence operator. Average density and average dynamic viscosity, $\bar{\rho}$ and $\bar{\mu}$ respectively, of the liquid-gas mixture (humid air and liquid water at the cathode; humid hydrogen and liquid water at the anode) is calculated based on liquid water volume fraction s. Namely, average density and average viscosity are given as $\bar{\rho} = s\rho_l + (1-s)\rho_g$ and $\bar{\mu} = s\mu_l + (1-s)\mu_g$ respectively, where subscripts l and g denote liquid water and gas (air in cathode or hydrogen in anode) respectively.

In particular, the proposed homogenized two-phase approach deals with the gas-liquid mixture as an single phase fluid, hence its continuity is ensured by $\frac{\partial \bar{\rho}}{\partial t} + \nabla \cdot (\bar{\rho}\mathbf{v}) = 0$. No phase change in the gas channels is considered.

Since many different species are involved in diffusion, the Fickian diffusion model, where diffusion flux of species is proportional to their concentration gradient neglecting interaction between species, is no longer applicable. Therefore the Maxwell-Stefan equations [1] are applied, namely

$$\sum_{\substack{k=1 \\ l \neq k}}^{N} \frac{X_k X_l}{D_{kl}} (\mathbf{V}_l - \mathbf{V}_k) = \nabla X_k \tag{2}$$

where N denotes number of considered species (oxygen and water vapour in cathode; hydrogen and water vapour in anode) $X_{k,l}$ are molar fractions of species k and l respectively, $\mathbf{V}$ is diffusion velocity of considered species. The procedure of calculating binary diffusion coefficients D_{kl} is presented in [1] depending on molar fraction and molar mass of considered species.

Heat transfer is modelled using the general diffusion equation. Due to relatively low heat conductivity of air and dominating convection, heat conduction in the gas channels is neglected. There is no heat source term for the gas channels, therefore:

$$\left(\frac{\partial}{\partial t} + \nabla \cdot \mathbf{v}\right) \bar{\rho} h = 0 \tag{3}$$

where h is sensible enthalpy.

Bi-polar plates (BPP)

The electric charge (electrons) in BPP is transferred between the terminal (connector to the external circuit) and BPP – GDL contact surface. The electric current model takes the time dependent Laplacian form:

$$\left(\frac{\partial}{\partial t} + \sigma_{\text{eff}}^{\text{BPP}} \nabla^2\right) \phi^{\text{BPP}} = 0\,, \tag{4}$$

where ∇^2 is Laplacian operator given as $\nabla^2 = \frac{\partial^2}{\partial x^2} + \frac{\partial^2}{\partial y^2} + \frac{\partial^2}{\partial z^2}$.

The electric potential and effective electrical conductivity in the bi-polar plate are denoted by ϕ^{BPP} and $\sigma_{\text{eff}}^{\text{BPP}}$, respectively. There are no electric charge sources ($S=0$) or convective terms ($\mathbf{v}=\mathbf{0}$) in BPP.

The heat transfer in the BPP is modelled by the diffusion equation as follows:

$$\frac{\partial}{\partial t}(\rho^{BPP} h) + k^{BPP} \nabla^2 T = S_h^{BPP} \tag{5}$$

where ρ^{BPP} and k^{BPP} are physical parameters of the BPP material, namely density and thermal conductivity, respectively; h is enthalpy of BPP and ∇T is the temperature gradient in BPP. Since the thermal conductivity is not dependent on spatial geometry, the k^{BPP} term is excluded from the divergence operator, hence the Laplacian operator (∇^2) appears. The volumetric source term S_h^{BPP} represents the Joule heating and depends on the local electric current and electrical conductivity as follows:

$$S_h^{BPP} = \frac{i^2}{\sigma_{eff}^{BPP}} \tag{6}$$

where i *is* the magnitude of the local electric current $\mathbf{i}$, calculated according to Ohm's law:

$$\mathbf{i} = \sigma_{eff}^{BPP} \nabla \phi_{eff}^{BPP}\,. \tag{7}$$

Gas diffusion, microporous and catalyst layers (GDL, MPL and CL)

The CFD approach does not allow for exact modelling of the solid structure of porous layers – carbon fibres for GDL, or noble metal catalyst (on carbon support) particles for MPL and CL. According to the Darcy approximation, where the flow velocity $\mathbf{v}$ is directly proportional to pressure gradient ∇p, permeability of the porous media K and inversely proportional to fluid dynamic viscosity μ and material porosity ε, namely

$$\mathbf{v} = -\frac{K}{\mu\varepsilon}\nabla p\,. \tag{8}$$

The solid structure of porous media is assumed homogenous and described by a scalar parameter – namely the average porosity ε. The appropriate transport parameters are expressed as functions of the average porosity. The superscripts *GDL* and *CL* indicate the parameters corresponding to GDL and CL, respectively.

Using the Darcy modification, the N-S equation (1) reads

$$\frac{\partial}{\partial t}(\bar{\rho}\varepsilon\mathbf{v}) + \nabla\cdot(\bar{\rho}\varepsilon\mathbf{v}\mathbf{v}) = \nabla\cdot(\bar{\mu}\varepsilon\mathbf{v}) - \varepsilon\nabla p + S_u \tag{9}$$

where S_u is a body force source term considering the viscous resistance of the fluid flowing through the porous layer:

$$S_u = -\frac{\bar{\mu}}{K}\varepsilon^2\mathbf{v} \tag{10}$$

where K is the permeability of the porous layer.

The conservation of gas species in GDL, MPL and CL is modified by homogenous porosity

$$\frac{\partial(\varepsilon C_k)}{\partial t} + \nabla\cdot(\varepsilon C_k\mathbf{v}) + \nabla\cdot(D_k^{eff}\nabla \mathrm{C_k}) = S_s^k \tag{11}$$

where S_s^k is a source of species k. D_k^{eff} is the effective diffusion coefficient in porous material:

$$D_k^{eff} = \frac{\varepsilon}{\tau}D_k \tag{12}$$

where τ is tortuosity. However, if the tortuosity factor is not known, it is possible to apply the Bruggemann approximation:

$$D_k^{eff} = \varepsilon^{1.5}D_k \tag{13}$$

where D_k is the gas species diffusivity computed according to multicomponent diffusion [1].

The sink terms for reactant species, S_s^k, take non-zero values only in the CL, where hydrogen (H_2) and oxygen (O_2) are consumed. The sink terms for H_2 and O_2 are given as:

$$S_s^{O_2} = -\frac{M_{O_2}}{4F}i_c \tag{14}$$

$$S_s^{H_2} = -\frac{M_{H_2}}{2F}i_a \tag{15}$$

where F is the Faraday constant, M_k is molecular weight of species k, and i_a and i_c are anode and cathode currents, respectively. The negative term on the right hand side of equations (14) and (15) denotes consumption of reactants. The constants "2" and "4" in the denominators of equations (14) and (15) represent the number of electrons taking part in the redox reactions: Hydrogen Oxidation Reaction (HOR) in anode and Oxygen Reduction Reaction in cathode, namely

$$\mathrm{HOR:}\quad H_2 \xrightarrow{Pt} 2H^{+1} + 2e^- \tag{16}$$

$$\mathrm{ORR:}\quad \frac{1}{2}O_2 \xrightarrow{Pt} \frac{1}{2}(2O^{-2} - 4e^-) \tag{17}$$

where superscripts correspond to electric charge and e^- is electron (negative charge).

Water is produced in dissolved form therefore the water vapour source term corresponds to mass exchange between water dissolved in the ionomer and water vapour and evaporation/condensation terms (S_{gd} and S_{gl}, respectively).

$$S_s^{H_2O} = -S_{gd} - S_{gl} \tag{18}$$

The term S_{gd} corresponding to the mass exchange between water vapour and dissolved water is given in equation (42). The evaporation/condensation term is given as:

$$S_{gl} = \begin{cases} \frac{M_{H_2O}}{RT}\gamma_{gl}\varepsilon s D_{gl}\, p \ln\left(\frac{p - p_{sat}}{(1 - X_{H_2O})p}\right) & \text{for} \quad X_{H_2O}\, p \le p_{sat} \quad \text{(evaporation)} \\ \frac{M_{H_2O}}{RT}\gamma_{gl}\varepsilon(1-s) D_{gl}\, p \ln\left(\frac{p - p_{sat}}{(1 - X_{H_2O})p}\right) & \text{for} \quad X_{H_2O}\, p > p_{sat} \quad \text{(condensation)} \end{cases} \tag{19}$$

where X_{H_2O} is mole fraction of water vapour, p is absolute gas pressure and p_{sat} is saturation vapour pressure, γ_{gl} is average surface of liquid water droplet and the D_{gl} term derives from an empirical formula depending on the gas (air or hydrogen) as follows:

$$D_{gl} = \begin{cases} 0.365 - 4\left(\frac{T}{343}\right)^{2.334}\left(\frac{p_0}{p}\right) & \text{for cathode} \\ 1.79 - 4\left(\frac{T}{343}\right)^{2.334}\left(\frac{p_0}{p}\right) & \text{for anode} \end{cases} \tag{20}$$

where T is gas temperature and p_0 is a reference pressure equal to an atmospheric pressure of 0.1MPa.

The heat transfer in GDLs and CLs is modelled by the diffusion equation modified for a homogenized porous medium:

$$\underbrace{\frac{\partial}{\partial t}(\varepsilon\bar{\rho}h)}_{\text{fluid}} + \underbrace{\frac{\partial}{\partial t}(\rho_{\text{GDL,CL}}h)}_{\text{solid structure}} + \underbrace{\nabla\cdot((1-\varepsilon)\bar{\rho}\mathbf{v}h)}_{\text{fluid}} = \underbrace{k^{GDL,CL}\nabla^2 T}_{\text{solid structure}} + S_h \tag{21}$$

- where $\rho_{GDL,CL}$ is an average (accounting volume of pores) density of the porous layer. S_h is the heat source term, which takes into account the Joule heat produced by transfer of current;
- the heat of water condensation/evaporation; *and*
- the reaction heat due to the hydrogen oxidation reaction in the cathode catalyst layer.

$$S_h = \begin{cases} \frac{i^2}{\sigma_{eff}^{GDL}} + h_{phase} & \text{for GDL} \\ \frac{i^2}{\sigma_{eff}^{CL}} + h_{phase} + h_{react} - i\eta & \text{for CL} \end{cases} \tag{22}$$

where h_{phase} is enthalpy change due to phase change (water condensation/evaporation), σ_{eff}^{GDL} and σ_{eff}^{CL} are electrical conductivities of gas diffusion and catalyst layers, respectively, and $k^{GDL,CL}$ is thermal conductivity of GDL or CL. In the cathode catalyst layer, there is another source term h_{react} corresponding to enthalpy change due to OOR while η is the overpotential.

The electric charge (electrons) is transferred between the CLs, where the electrochemical reactions occur on the triple phase boundary and the electrical terminals of the bi-polar plate. The electric current flow is modelled taking into account the homogenized porosity of both gas diffusion and catalyst layers, as follows:

$$\left(\frac{\partial}{\partial t} + \sigma_{\text{eff}}^{\text{GDL,CL}}\nabla^2\right)\Phi^{\text{GDL,CL}} = S_e \tag{23}$$

The source term S_e takes non-zero values only in the catalyst layer (where electrochemical reactions occur) and is equal to the generated electric current:

$$S_e = \begin{cases} 0 & \text{for GDL and MPL} \\ J_{an,cat} & \text{for CL} \end{cases} \quad (24)$$

where J is volumetric current density due to HOR or ORR. Subscripts an and cat correspond to the anode and cathode, respectively.

The difference between the phase potential of the solid BPP terminal (external boundary condition) and the phase potential of the membrane is the main driving force for the electrochemical reactions HOR and ORR.

The anode and cathode source terms $J_{an,cat}$ are given in general form by the well-known Butler-Volmer (B-V) reaction kinetics equation:

$$J_{an} = j_{an}^{ex}\left(\frac{X_{H_2}}{X_{H_2}^{ref}}\right)^{\gamma_{an}}\left[\exp\left(\frac{\alpha_{an}F\eta_{an}}{RT}\right) - \exp\left(\frac{-(1-\alpha_{an})F\eta_{an}}{RT}\right)\right] \quad (25)$$

$$J_{cat} = j_{cat}^{ex}\left(\frac{X_{O_2}}{X_{O_2}^{ref}}\right)^{\gamma_{cat}}\left[\exp\left(\frac{-\alpha_{cat}F\eta_{cat}}{RT}\right) - \exp\left(\frac{(1-\alpha_{cat})F\eta_{cat}}{RT}\right)\right] \quad (26)$$

where:

- F and R are Faraday and universal gas constants;
- T is the local temperature;
- j_{an}^{ex} and j_{cat}^{ex} are exchange current densities [A m^{-3}] for anode and cathode catalysts, respectively, given in Appendix B, Table 10. Note that Electro-Chemical Surface Area (ECSA, defined as an active catalyst area surface per volume) is already accounted for by

  $$j_{an,cat}^{ex} = j_{an,cat}^{ref}\zeta_{an,cat} \quad (27)$$

  where $j_{an,cat}^{ref}$ is reference current density per active catalyst area [A m^{-2}], ζ is ECSA [m^{-1}];
- X_{H_2} and X_{O_2} are hydrogen and oxygen local concentrations [mole m^{-3}]. The reference values of $X_{H_2}^{ref}$ and $X_{O_2}^{ref}$ are given in Appendix B, Table 10 and correspond to reactant concentrations at NTP[3] conditions;
- Anode and cathode concentration exponents are denoted by γ_{an} and γ_{cat}, respectively. The values of these constants are considered as fitting parameters, however $\gamma_{an}=0.5$ and $\gamma_{cat}=1.0$ are mentioned in many papers, i.e. [2];
- α_{an} and α_{cat} are anode and cathode exchange coefficients. The exchange coefficient α is related to reaction symmetry factor β, as follows [3]:

  $$\alpha = n\beta \quad (28)$$

  where n is the number of electrons taking part in the reaction:

  $$\frac{1}{2}H_2 \rightarrow H^+ + \bar{e}, \qquad \frac{1}{2}O_2 \rightarrow O^{2-} - 2\bar{e} \quad (29)$$

  According to [3], PEM fuel cell reactions are symmetric ($\beta=0.5$), hence the values of anode and cathode exchange coefficients are taken as $\alpha_{an}=0.5$ and $\alpha_{cat}=1.0$; *and*
- η_{an} and η_{cat} are anode and cathode overpotentials, respectively, defined as follows:

  $$\eta_{an} = \phi_{mem} - \phi_{sol} - U_{an}^0, \qquad \eta_{cat} = \phi_{mem} - \phi_{sol} - U_{cat}^0 \quad (30)$$

[3] Normal Temperature and Pressure: 20°C (293.15 K) and 1 atm (101.325 kPa).

where ϕ_{mem} and ϕ_{sol} are potentials of the electrolyte and carbon support in the appropriate catalyst layer. The half-potentials U_{an}^{0} and U_{cat}^{0} are defined as follows:

$$U_0^{an} = -\frac{RT}{2F}\ln\left(\frac{p_{H_2}}{p_0}\right) \quad (31)$$

$$U_0^{ca} = E_0 + \frac{RT}{4F}\ln\left(\frac{p_{O_2}}{p_0}\right) - \frac{RT}{2F}\ln\left(\frac{p_{H_2O}}{p_{sat}}\right) \quad (32)$$

where p denotes pressure, while subscripts H_2, O_2 and H_2O refer to the partial pressure of the gas species, p_0 is a reference pressure equal to 0.1MPa, p_{sat} is the saturation pressure of water vapour. Note, the total pressure is the sum of the partial pressure of all species present less the saturation pressure of water.

E_0 corresponds to the reversible potential of fuel cell reactions, defined as:

$$E_o = -\frac{\Delta G}{2F} \quad (33)$$

where ΔG is change of free Gibbs energy, which at 80°C is equal to -2.262 x 10^5 [J $mole^{-1}$]. Therefore, at an operating temperature of 80°C, the reversible potential E_0 is equal to 1.172 [V].

The transport of liquid water through GDL, MPL and CL follows the equation:

$$\frac{\partial}{\partial t}(\varepsilon\rho_l s) = \nabla\cdot\left(\frac{\rho_l K K_r}{\mu_l}\nabla p_l\right) + \nabla\cdot\left(D_m^{eff}\nabla s\right) - S_{ld} + S_{gl} \quad (34)$$

where, ε is porosity, ρ_l and μ_l are liquid water density and viscosity respectively, s is liquid water saturation, K and K_r are absolute permeability of the porous layer and relative permeability due to saturation effect, respectively, S_{ld} is liquid water uptake by the membrane, D_m^s is an effective diffusion coefficient for liquid water.

The left hand side term in equation 34 corresponds to the dynamic inertial term while the right hand side refers to the steady state transport of liquid water. The consecutive terms in the right hand side refer to:

- $\frac{\rho_l K K_r}{\mu_l}\nabla p_l$ which is a liquid water flux due to pressure difference and
- $D_m^{eff}\nabla s$ which is a liquid water flux due to saturation gradient.

The liquid water pressure is a sum of gas phase pressure p and capillary pressure p_c, namely:

$$p_l = p + p_c \quad (35)$$

The relative water permeability of porous layer due to liquid water saturation is approximated as:

$$K_r = s^b \quad (36)$$

where exponent b is a user-defined constant (assumed $b=3.0$)[1]. The effective diffusion coefficient in the membrane D_m^{eff} is given in equation (12).

Membrane

Transport of H^+ ions in the ionomer (membrane and CL)

Due to the fact that H^+ ion transport takes place through the membrane, but between the anode and cathode catalyst layers, the ionomer volume fraction in both catalyst layers is taken into consideration.

The conservation equation for electrical charge in the membrane is expressed as follows:

$$\nabla\cdot\left(\sigma_{mem}^{\text{eff}}\nabla\phi_{mem}\right) = 0 \quad (37)$$

where, $\sigma_{mem}^{\text{eff}}$ is the effective ionic conductivity of the membrane and ϕ_{mem} is the membrane potential. The effective ionic conductivity is dependent on membrane liquid water content, λ, and temperature, T, and is given as follows [4]:

$$\sigma_{mem}^{\text{eff}}(\lambda, \mathrm{T}) = \Gamma(0.514\lambda - 0.326)\exp\left(E_i\left(\frac{1}{303} - \frac{1}{T}\right)\right) \tag{38}$$

E_i stands for activation energy for temperature correction. Γ factor is defined as follows:

$$\Gamma = \begin{cases} 1 & \text{in membrane} \\ \frac{\epsilon_a}{\tau_a} & \text{in anode catalist} \\ \frac{\epsilon_c}{\tau_c} & \text{in cathode catalist} \end{cases} \tag{39}$$

where, ϵ and τ refer to volume fraction and tortuosity of ionomer in anode (subscript *a*) and cathode (subscript *c*) catalyst layers, respectively.

Water transport though the membrane

In PEM fuel cell water exist in three phases, namely:

- water vapour as humidification of anode and cathode gases;
- liquid water, considered as fine homogenous mist; *and*
- dissolved water in the membrane ionomer.

Transport equation of dissolved water in the ionomer

Dissolved water phase exists in the ionomer in both anode and cathode catalyst layers and in the membrane. The transport of dissolved water, both ways due to osmotic drag and back diffusion due to concentration gradient, follows the formula [4]:

$$\frac{\partial}{\partial \mathrm{t}}\left(\epsilon_i M_{H_2O}\frac{\rho_l}{EW}\lambda\right) + \nabla\cdot\left(\mathbf{i}\frac{n_d}{F}M_{H_2O}\right) = \nabla\cdot\left(M_{H_2O}D_\lambda\nabla\lambda\right) + S_\lambda + S_{gd} + S_{ld} \tag{40}$$

where:

- λ is a dimensionless water content defined as the number of water molecules per number of charge sides ($-SO_3^-H^+$)[2,5,6];
- ϵ_i is a dimensionless volume fraction of the ionomer (equal 1 for the membrane) [4];
- ρ_i is density of the dry ionomer [kg m^{-3}];
- EW is membrane equivalent weight (weight per one acid site $-SO_3^-$) [kg mol^{-1}];
- M_{H_2O} is molecular weight of water [kg mol^{-1}];
- n_d is dimensionless osmotic drag coefficient;
- D_λ is diffusion coefficient of water content [mol s^{-1}];
- S_λ is dissolved water production rate in cathode catalyst due to ORR reaction [kg s^{-1}], equals 0 in anode;
- S_{gd} is mass change rate between gas and dissolved phases [kg s^{-1}];
- S_{ld} is mass change rate between liquid and dissolved phases [kg s^{-1}]; *and*
- $\mathbf{i}$ is ionic current [A] calculated as $\mathbf{i} = -\sigma_{mem}^{eff}\nabla\phi_{mem}$

Source terms on the right hand side of equation 40 are defined as follows:

$$S_\lambda = \frac{M_w^{H_2O}}{2F} j_{cat} \tag{41}$$

$$S_{gd} = (1 - s^\theta)\gamma_{gd} M_w^{H_2O} \frac{\rho_i}{EW} (\lambda_{eq} - \lambda) \tag{42}$$

$$S_{ld} = s^\theta \gamma_{ld} M_w^{H_2O} \frac{\rho_i}{EW} (\lambda_{eq} - \lambda) \tag{43}$$

where j_{cat} is current density in the cathode catalyst layer, s is liquid water saturation, θ is user defined constant, γ_{gd} and γ_{ld} are gas to dissolved and liquid to dissolved mass exchange rate constants for water. The equilibrium water content is given as follows [4]:

$$\lambda_{eq} = 0.3 + 6a(1 - \tanh(a - 0.5)) + 0.69(\lambda_{a=1} - 3.52)a^{0.5}\left(1 + \tanh\left(\frac{a-0.89}{0.23}\right)\right) + s(\lambda_{s=1} - \lambda_{a=1}) \tag{44}$$

where a stands for water activity.

$$a = \frac{x_{H_2O}\, p}{p_{sat}} \tag{45}$$

where x_{H_2O} is mole fraction of water vapour, p is absolute gas pressure and p_{sat} is saturation vapour pressure. Parameters $\lambda_{s=1}$ and $\lambda_{a=1}$ in equation 44 are user-defined constants equal to 16.8 and 9.2, respectively [5].

Diffusivity of the water content in the membrane is given as follows [4]:

$$D_\lambda = \frac{\rho_i}{EW} 4.1 \cdot 10^{-10} \left(\frac{\lambda}{25}\right)^{0.15} \left(1 + \tanh\left(\frac{\lambda - 2.5}{1.4}\right)\right) \tag{46}$$

The value of the osmotic-drag coefficient, n_d, is given as [7]:

$$n_d = \frac{2.5}{22}\lambda \tag{47}$$

However, other researchers provide a bi-linear osmotic drag coefficient relation to water content, λ, or simply a constant value equal to n_d=*1.0* [8].

Transport of liquid water due to concentration, pressure and temperature difference

The transport of liquid water through the membrane follows the equation:

$$\frac{\partial}{\partial t}\left(\epsilon_{mem}^{liquid} \rho_l s\right) = \nabla \cdot \left(\frac{\rho_l K K_r}{\mu_l} \nabla p_l\right) + S_{ld} \tag{48}$$

where, ϵ_{mem}^{liquid} is the volume fraction of membrane that could be occupied by liquid water, ρ_l and μ_l are liquid water density and viscosity, respectively, K and K_r are absolute and relative water permeability of the membrane, respectively, and S_{ld} is the uptake of liquid water by the membrane defined in equation (43).

The liquid water pressure is a sum of gas phase pressure, p, and capillary pressure, p_c, namely:

$$p_l = p + p_c \tag{49}$$

The relative water permeability of the membrane is a function of membrane water content:

$$K_r = \left(\frac{\frac{M_{H_2O}}{\rho_i}\lambda_{s=1} + \frac{EW}{\rho_i}}{\frac{M_{H_2O}}{\rho_i}\lambda + \frac{EW}{\rho_i}} \frac{\lambda}{\lambda_{s=1}}\right)^2 \tag{50}$$

Heat transfer

The heat transfer in the membrane is modelled as follows:

$$\frac{\partial}{\partial t}\left(\frac{\rho_i}{EW}h\right) + k_{mem}\nabla^2 T = S^h_{mem} \tag{51}$$

where ρ_i and k_{mem} are physical parameters of the membrane material, namely density and thermal conductivity, respectively, h is enthalpy of the membrane and ∇T is the temperature gradient. Since the thermal conductivity is not dependent on spatial geometry, the k^{BPP} term is excluded from the divergence operator hence the Laplacian operator (∇^2) appears. The volumetric source term, S_h^{BPP}, represents the Joule ohmic heating and depends on the local protonic current, i, and protoic conductivity as follows:

$$S^h_{mem} = \frac{i_p^2}{\sigma^{eff}_{mem}} \tag{52}$$

The local protonic current, i_p, and its magnitude, i_p, is proportional to the protonic potential gradient $\nabla\Phi_{mem}$ and is calculated according to Ohm's law

$$\mathbf{i_p} = \sigma^{eff}_{mem}\nabla\phi_{mem} \tag{53}$$

References

[1] E.L. Cussler, Diffusion. Mass Transfer in Fluid Systems, Cambridge University Press, Cambridge, 2009.

[2] A.Z. Weber, R.L. Borup, R.M. Darling, P.K. Das, T.J. Dursch, W. Gu, D. Harvey, A. Kusoglu, S. Litster, M.M. Mench, R. Mukundan, J.P. Owejan, J.G. Pharoah, M. Secanell, I. V Zenyuk, J. Electrochem. Soc. 161 (2014) F1254.

[3] R.F. Mann, J.C. Amphlett, B.A. Peppley, C.P. Thurgood, J. Power Sources 161 (2006) 775.

[4] H. Wu, X. Li, P. Berg, Electrochim. Acta 54 (2009) 6913.

[5] T.E. Springer, M.S. Wilson, S. Gottesfeld, J. Electrochem. Soc. 140 (1993) 3513.

[6] A.Z. Weber, J. Newman, Adv. Fuel Cells 1 (2007) 47.

[7] T.E. Springer, T.A. Zawodzinski, S. Gottesfeld, J. Electrochem. Soc. 138 (1991) 2334.

[8] T. Berning, M. Odgaard, S.K. Kær, J. Power Sources 196 (2011) 6305.

Appendix B Reference test case 1 for PEMFC single cell

Computational geometry

To simplify the numerical solution, the "single serpentine cell" is approximated by a "single straight channel" of equivalent channel length. The cross-sectional area of the anode and cathode flow channels is 1.5 mm^2 – the channel width is 1 *mm* and the height of the channel is 1.5 *mm*. The width of the bi-polar plate ribs is also 1 *mm*. The length of the gas channels is 1250 *mm*, which corresponds to the total length of the gas channels in a serpentine configuration representing a 25 cm^2 active area.

Due to vertical symmetry planes of the gas channels and bi-polar plate, only half of the gas channel and half of the rib are modelled. The geometry of the numerical model is presented in Figure 6. The computational model covers half of the fuel cell active area, namely 12.5 cm2.

The gas diffusion layers on the cathode and anode sides are the same and of 200 μm thickness according to SGL®GDL24BC data sheets. The catalyst layers and the microporous layers are 20 μm thick on both sides. The membrane is assumed to be 20 μm in thickness.

Figure 6 Computational domain.

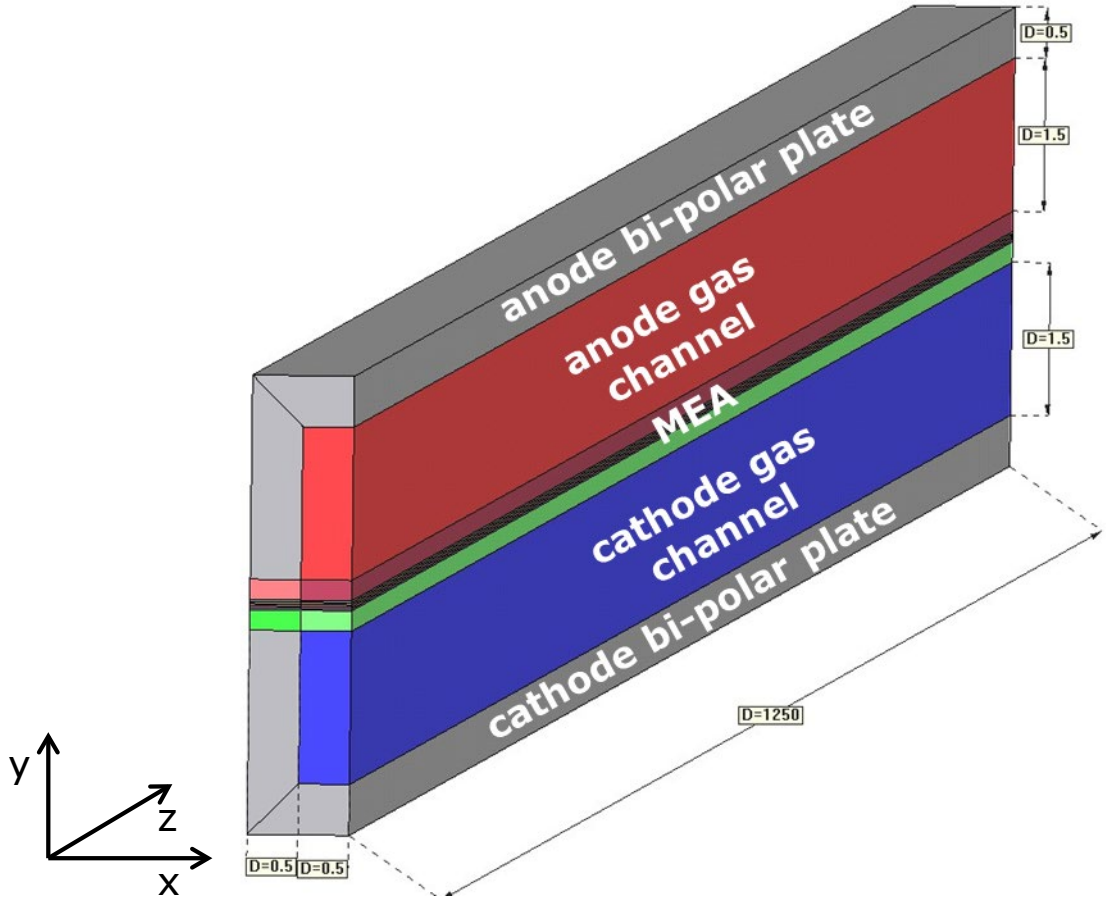

Source: JRC, 2017

Model assumptions

The following working assumptions were made:

- The flow of reactant gases (air and hydrogen) within the fuel cell is counter flow;
- The open circuit voltage V^{OC} is estimated on the basis of the Nernst equation. If this is not possible, V^{OC} should be assumed as a constant input value; *and*
- The electrical boundary conditions at the anode and cathode bi-polar plate terminals are expressed as current density related to the catalyst area.

External boundary conditions

The fuel cell model boundary conditions are assumed as follows (Figure 7).

- The top and bottom surfaces of the bi-polar plates are assumed to be the fuel cell electric terminals. The potential on the anode bi-polar plate terminal is set to 0 *V* while the current or potential is applied to the cathode bi-polar plate terminal, depending on the set operation mode, namely galvanostatic or potentiostatic.
- A nominal operating temperature is applied to both terminals.
- Symmetry boundary conditions are applied on the fuel cell model symmetry plane.
- The inlet flow rates of oxidant (air) and fuel (hydrogen) are calculated according to the stoichiometry regime.
- The inlet pressure is equal to the operating pressure. However, if it is not possible to apply inlet pressure, the outlet pressure could be specified instead.
- There are no flux conditions (species, temperature and electric charge) on the solid surfaces at other external walls of the fuel cell model.

External boundary conditions are presented in Figure 7 and Table 4 while operating conditions are given in Table 4. Subsequent tables show the physical properties of fuel cell component materials, air and hydrogen.

Figure 7 External boundary conditions.

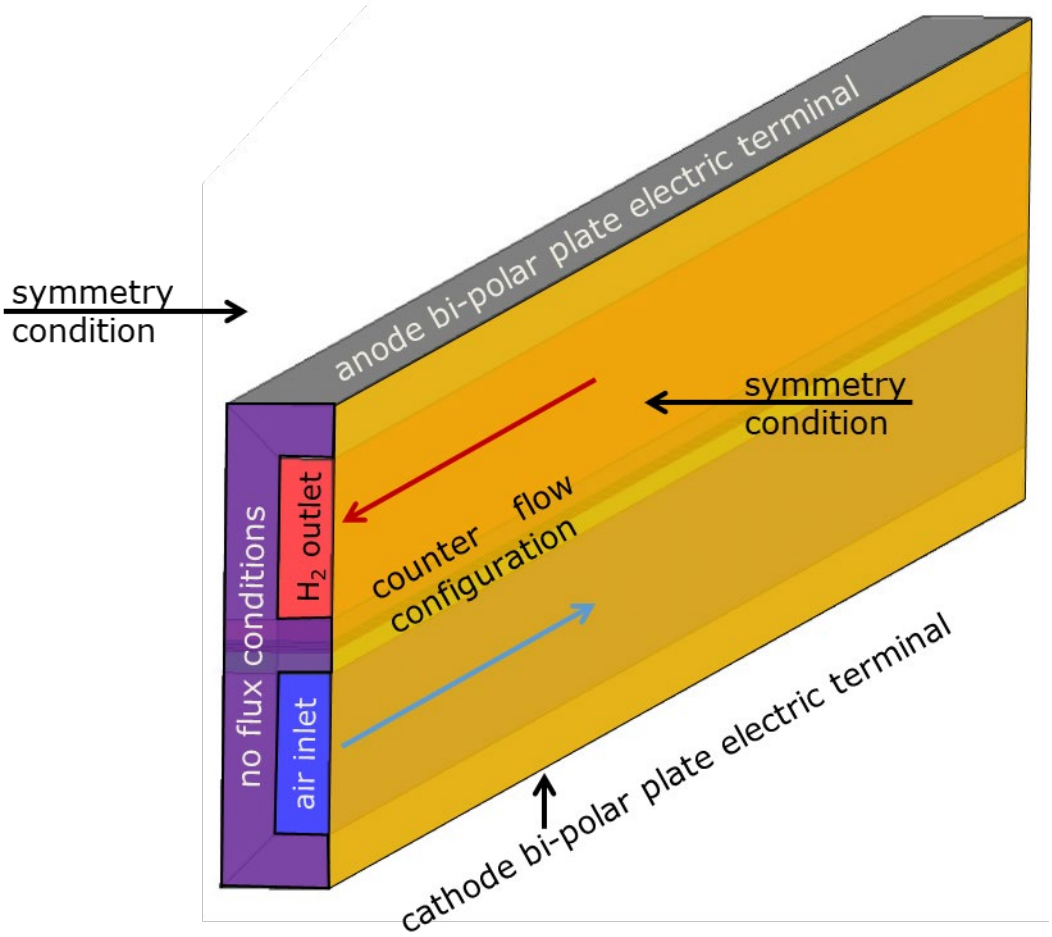

Source: JRC, 2017

Table 4 External boundary conditions.

Location	Boundary condition
Inlet of the anode gas channel (hydrogen)	Mass flow rate of fuel (hydrogen + water vapour): $Q_{H_2} = \overline{Q_{H_2}}$ Mole fractions of fuel species: $C[H_2] = \overline{C[H_2]}, \quad C[H_2O] = \overline{C_{anode}[H_2O]}$ Temperature of inlet gas: $T = \bar{T}$
Outlet of the anode gas channel	Outlet pressure: $p = \bar{p}_{anode}$
Inlet of the cathode gas channel (air)	Mass flow rate of humid air (air+water vapour): $Q_{air} = \overline{Q_{air}}$ Mole fraction of air species: $C[O_2] = \overline{C[O_2]}, \quad C[H_2O] = \overline{C_{cathode}[H_2O]}$ Temperature of inlet gas: $T = \bar{T}$
Outlet of the cathode gas channel	Outlet pressure: $p = \overline{p_{cathode}}$
Symmetry planes, orange surfaces in Figure 7	Zero current flux normal to the symmetry plane: $\frac{\partial \mathrm{j}}{\partial \mathrm{x}} = 0$ Zero velocity normal to the symmetry plane: $\mathrm{V_x} = 0$ Zero species concentration gradients normal to the symmetry plane: $\frac{\partial \mathrm{C[H_2]}}{\partial \mathrm{x}} = 0, \quad \frac{\partial \mathrm{C[H_2O]}}{\partial \mathrm{x}} = 0, \quad \frac{\partial \mathrm{C[O_2]}}{\partial \mathrm{x}} = 0$ Zero temperature gradient, normal to the symmetry plane: $\frac{\partial \mathrm{T}}{\partial \mathrm{x}} = 0$
End of model, green surfaces in Figure 7	Zero current flux normal to the boundary: $\frac{\partial \mathrm{j}}{\partial \mathrm{z}} = 0$ No slip velocity constraint: $\mathrm{V} = [0 \quad 0 \quad 0]^{\mathrm{T}}$ Zero species concentration gradient normal to the boundary: $\frac{\partial \mathrm{C[H_2]}}{\partial \mathrm{z}} = 0, \quad \frac{\partial \mathrm{C[H_2O]}}{\partial \mathrm{z}} = 0, \quad \frac{\partial \mathrm{C[O_2]}}{\partial \mathrm{z}} = 0$ Zero temperature gradient normal to the boundary: $\frac{\partial \mathrm{T}}{\partial \mathrm{z}} = 0$
Anode bi-polar plate terminal	Potential equal zero: $\Phi = 0$ Temperature: $T = \bar{T}$
Cathode bi-polar plate terminal	Prescribed electric current density: $\mathbf{j} = \bar{\mathbf{j}}$ Temperature: $T = \bar{T}$

Source: JRC, 2017

Table 5 Operating Conditions

	Parameter	Operating conditions		
		Symbol	Unit	Setting
	Nominal cell operating temperature	T_{cell}	K	353
ANODE	Fuel gas inlet temperature	$T_{fuel,in}$	K	353
	Fuel gas inlet humidity RH	$RH_{fuel,in}$	%	50
	Fuel gas inlet pressure (absolute)	$P_{fuel,in}$	kPa	250
	Fuel inlet stoichiometry	λ_{H2}	–	1.3
CATHODE	Oxidant gas inlet temperature	$T_{air,in}$		353
	Oxidant gas inlet humidity	$RH_{Ox,in}$	%	30
	Oxidant inlet pressure (absolute)	$P_{Ox,in}$	kPa	230
	Oxidant inlet stoichiometry	λ_{Ox}	–	1.5
Minimum current density for stoichiometry operation		J_{min}	A cm^{-2}	0.2

Source: JRC, 2017

The simulation of the fuel cell operating at a current density of 0.2 Acm^{-2} and higher, follows the stoichiometry regime, i.e. the amount of supplied oxidant (air) and fuel (hydrogen) is directly proportional to the applied current density. For low current densities of up to 0.2 Acm^{-2}, the constant flow rates of the supplied gases are assumed to be equal to the flow rate corresponding to the current density 0.2 Acm^{-2}.

The inlet mas flow rate of the supplied gases is calculated according to the formula:

$$Q_x = \frac{M_x J A \lambda_x}{z_x F \phi_x}$$

where subscript x corresponds to hydrogen or air. M_x is the molar mass, J is the applied current density, A is the active area of the catalyst layer, z_x is the coefficient corresponding to the number of atoms taking part in the reactions, F is Faraday constant, ϕ_x is the volumetric content of hydrogen or oxygen in the supplied gases. The values of the quantities are given in Table 6.

Table 6 Properties of reactant gases for calculation of the inlet mass flow rates

	air	hydrogen
***Mx* [kg mol^{-1}]**	28.186e-3	3.509e-3
z	4	2
ϕ^x [%]	19.66	90.57

Source: JRC, 2017

The composition of inlet gases (mole fractions of gas species) is defined for the nominal operating fuel cell temperature. The 30% RH air, the oxidant gas, is composed as follows [mole fractions]: $\bar{C}$[O_2]=0.1966, $\bar{C}$ [H_2O]=0.0615 and $\bar{C}$ [N_2]=0.7419, while the fuel (RH 50%) is composed of $\bar{C}$ [H_2]=0.9057 and $\bar{C}$ [H_2O]=0.0943 [mole fractions].

Physical properties

The physical constants and parameters of the fuel cell used in the current computations are listed in Tables 7 to 13.

Table 7 Physical properties of inlet gases at operating conditions

Parameter	Unit	H2	O2	N2	H2O (vapour)
Specific heat	J kg-1 K-1	14.43e3	0.928e3	1.041e3	1.88e3
Thermal conductivity	W m-1 K-1	0.253	0.031	0.030	0.025
Viscosity	Kg m-1 s-1	8.41e-6	2.34e-5	2.01e-5	1.30e-5
Molecular weight	kg mol-1	2.02e-3	31.99e-3	28.01e-3	18.01e-3

Source: JRC, 2017

Table 8 Properties of bi-polar plates

Parameter	Unit	Value
Specific heat	J kg^{-1}K^{-1}	708
Thermal conductivity	W m^{-1}K^{-1}	10.0
Electrical conductivity	Ohm^{-1}m^{-1}	1.0e5
Density	kg m^{-3}	2100

Source: JRC, 2017

Table 9 Properties of anode and cathode Gas Diffusion Layers

Parameter	Unit	Value	
		Under the channel	Under the rib
Specific heat	J $kg^{-1}K^{-1}$	708	708
Thermal conductivity*	W $m^{-1}K^{-1}$	0.83	0.95
Electrical conductivity*	$Ohm^{-1}m^{-1}$	184	195
Density*	kg m^{-3}	422	850
Thickness	µm	200	200
Porosity	%	70	50
Gas permeability	m^2	6.74e-14	2.50e-14
Contact angle	deg	112	112

* effective value, porosity is taken into account

Source: JRC, 2017

Table 10 Properties of anode and cathode Microporous Layers

Parameter	Unit	Value
Specific heat	J $kg^{-1}K^{-1}$	708
Thermal conductivity*	W $m^{-1}K^{-1}$	1.5
Electrical conductivity*	$Ohm^{-1}m^{-1}$	2.0e3
Density*	kg m^{-3}	1260
Thickness	µm	20
Porosity	%	40
Gas permeability	m^2	3.33e-15
Contact angle	deg	112

* effective value due to porosity is taken into account

Source: JRC, 2017

Table 11 Properties of anode and cathode Catalyst Layers

Parameter		**Unit**	**Value**
Specific heat		$J\ kg^{-1}K^{-1}$	680
Thermal conductivity*		$W\ m^{-1}K^{-1}$	1.7
Electrical conductivity*		$Ohm^{-1}m^{-1}$	5.0e3
Density*		$kg\ m^{-3}$	1350
Thickness		µm	20
Porosity		%	38
Volume fraction of ionomer		%	25
Ionomer tortuosity			1.5
Gas permeability		m^2	2.0e-15
Contact angle		deg	112
Catalyst loading	Anode	$mg\ cm^{-2}$	0.2
	Cathode		0.4
ECSA**	Anode	$m^2\ m^{-3}$	1.7e7
	Cathode		3.0e7

* effective value, porosity is taken into account
** ECSA – Electro-Chemical Surface Area

Source: JRC, 2017

Table 12 Properties of membrane.

Parameter	Unit	Value
Specific heat	J $kg^{-1}K^{-1}$	2000
Thermal conductivity*	W $m^{-1}K^{-1}$	0.2
Equivalent weight	-	1100
Thickness	µm	20
Protonic conductivity	S m^{-1}	$\kappa = (0.5139\lambda - 0.326)exp\left[1268\left(\frac{1}{303} - \frac{1}{T}\right)\right]$
Osmotic drag coefficient		$n_{drag} = \frac{2.5}{22}\lambda$
Water diffusivity in membrane	m^2 s^{-1}	$D_\lambda = \frac{\rho_i}{EW} 4.1 \cdot 10^{-10} \left(\frac{\lambda}{25}\right)^{0.15} \left(1 + \tanh\left(\frac{\lambda - 2.5}{1.4}\right)\right)$

Source: JRC, 2017

Table 13 Electrochemical parameters corresponding to Butler-Volmer reaction kinetics

Parameter	Unit	Value	
		Anode (H_2)	**Cathode (O_2)**
Exchange current density*	Am^{-3}	1.0e9	1.0e4
Reference specie concentration	mole m^{-3}	41.1	8.65
Concentration exponent		0.5	1
Exchange coefficient		0.5	1
Open circuit voltage	V	Eq. (1)	
Half-cell potentials	V	Eq. (2)	Eq. (3)

* The exchange current density takes into account the ECSA as well.

Source: JRC, 2017

$$E_o = -\frac{\Delta G}{2F} \quad (1)$$

$$U_0^{an} = -\frac{RT}{2F}\ln\left(\frac{p_{H_2}}{p_0}\right) \quad (2)$$

$$U_0^{ca} = E_0 + \frac{RT}{4F}\ln\left(\frac{p_{O_2}}{p_0}\right) - \frac{RT}{2F}\ln\left(\frac{p_{H_2O}}{p_{sat}}\right) \quad (3)$$

where R and F are gas and Faraday constants, $\ln(\cdot)$ is natural logarithm, T is temperature, ΔG is change of free Gibbs energy, p denotes pressure, while subscripts H_2, O_2 and H_2O refer to partial pressures of gas species, p_0 is a reference pressure equal to 0.1MPa, p_{sat} is the saturation pressure of water vapour.

Appendix C Reference test case 2 for catalyst layer examination

INTRODUCTION

The polarisation IV curve can be split into three regions of interest as shown in Figure 8, namely:

- Region I; Kinetics Region where electrochemical kinetics play a major role.
- Region II; Ohmic Region where the ohmic resistance of PEMFC components is the main source of voltage losses. In this region in particular, the membrane models will be evaluated.
- Region III; Transport Limitations Region where liquid water and properties of diffusion media are dominant.

Figure 8 Regions of interest

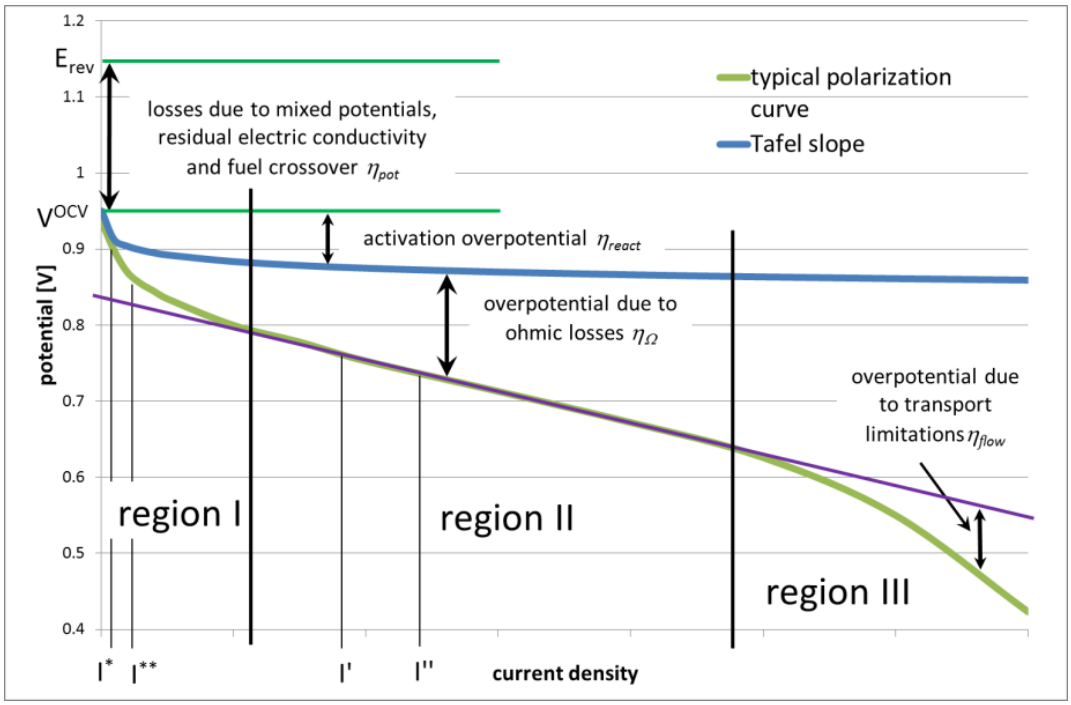

Source: JRC, 2017

In region I, electrochemical kinetics and catalyst layer properties play the dominant role in determining the polarisation curve. Therefore, in benchmarking test case 2, the geometry, boundary and operating conditions are adjusted accordingly to place emphasis on the modelling of the electrochemical kinetics.

Geometry

In an effort to simplify the numerical solution and to minimize the effects of gas flows on the fuel cell kinetics the "single straight channel" is considered. The cross-sectional area of the anode and cathode flow channels is 1.5 mm^2 with a channel width 1.0 mm and channel height of 1.5 mm. The width of the bi-polar plate ribs is also 1.0 mm. The length of the gas channels is equal to 80.0 mm, representing a 1.6 cm^2 active area. The length of the fuel cell model and operating conditions (Table 14) were assumed to minimize gradients of pressure, concentration of reactants and temperature within the fuel cell active area.

Due to vertical symmetry planes of the gas channels and bi-polar plate, only half of the gas channel and half of the rib are modelled. The geometry of the numerical model is presented in Figure 9. Therefore, the computational model covers half of the fuel cell active area, namely 0.80 cm^2.

The gas diffusion layers on the cathode and anode sides are the same having 200 μm thickness – according to SGL®GDL24BC data sheets. The catalyst layers and the microporous layers are 20 μm thick on both sides. The membrane is assumed to be 20 μm in thickness.

Figure 9 Computational domain for Region I – electrochemistry kinetics.

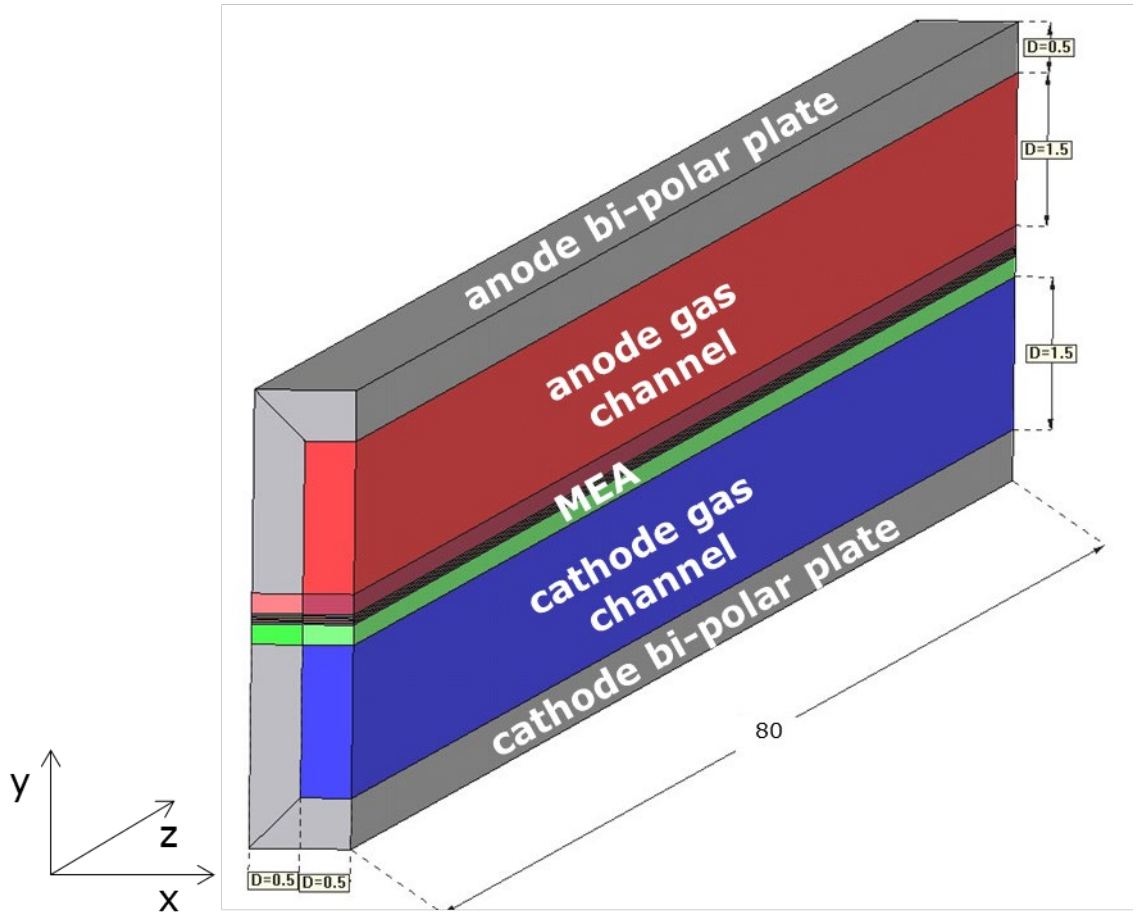

Source: JRC, 2017

Common Operating Conditions

The Common Operating conditions for electrochemical kinetics evaluation of the PEM fuel cell are listed in Table 14.

Table 14 Operating Conditions for benchmarking test case 2.

	Parameter	Operating conditions		Justification
		Unit	Setting	
	Nominal cell operating temperature	^{o}C	80	Typical temperature for PEM fuel cell operation
ANODE	Fuel gas inlet temperature	^{o}C	80	The same as cell operating temperature
	Fuel gas inlet humidity RH	%	100	To avoid drying out of the membrane
	Fuel gas inlet pressure (absolute)	bar	2.5	Ambient pressure to avoid pressure corrections in electrochemical parameters
	Fuel inlet stoichiometry	–	Constant flow equivalent to stoichiometry 10.0 @1 Acm^{-2}	To satisfy uniform distribution of species
CATHODE	Oxidant gas inlet temperature	^{o}C	80	The same as operating temperature
	Oxidant gas inlet humidity	%	100	To avoid drying out of the membrane
	Oxidant inlet pressure (absolute)	bar	2.3	To avoid pressure corrections
	Oxidant inlet stoichiometry	–	Constant flow equivalent to stoichiometry 10.0 @1 Acm^{-2}	To satisfy uniform distribution of species
Current density		Acm^{-2}	OCV* – 1.0	Only kinetics region of polarization curve

* if OCV conditions cannot be simulated, a current density of 5 $mAcm^{-2}$ should be applied.

Source: JRC, 2017

Gas composition and mass flow rates of supplied air and hydrogen for the 0.8cm^2 active area model are presented in Figure 9 and are listed in Table 15.

Table 15 Mass flow rates and gas composition of supplied gases

	Parameter	Setting	
ANODE	Total mass flow rate	kg s^{-1}	1.539E-7 *
	H_2 gas species	Mole fraction	0.811
	Water vapour	Mole fraction	0.189
CATHODE	Total mass flow rate	kg s^{-1}	3.314E-6 *
	O_2 gas species	Mole fraction	0.167
	H_2O gas species	Mole fraction	0.205

* mass flow rates are equivalent to 0.8cm^{-2} active area.

FUEL CELLS AND HYDROGEN
JOINT UNDERTAKING

European Commission

GETTING IN TOUCH WITH THE EU

In person

All over the European Union there are hundreds of Europe Direct information centres. You can find the address of the centre nearest you at: https://europa.eu/european-union/contact_en

On the phone or by email

Europe Direct is a service that answers your questions about the European Union. You can contact this service:

- by freephone: 00800 6 7 8 9 10 11 (certain operators may charge for these calls),

- at the following standard number: +32 22999696, or

- by electronic mail via: https://europa.eu/european-union/contact_en

FINDING INFORMATION ABOUT THE EU

Online

Information about the European Union in all the official languages of the EU is available on the Europa website at: https://europa.eu/european-union/index_en

EU publications

You can download or order free and priced EU publications from EU Bookshop at: https://publications.europa.eu/en/publications. Multiple copies of free publications may be obtained by contacting Europe Direct or your local information centre (see https://europa.eu/european-union/contact_en).

KJ-NA-30703-EN-N

The European Commission's science and knowledge service

Joint Research Centre

JRC Mission

As the science and knowledge service of the European Commission, the Joint Research Centre's mission is to support EU policies with independent evidence throughout the whole policy cycle.

EU Science Hub

ec.europa.eu/jrc

@EU_ScienceHub

EU Science Hub - Joint Research Centre

Joint Research Centre

EU Science Hub

Publications Office of the European Union

doi:10.2760/291664

ISBN 978-92-76-37770-2